Optics & Laser Technology 170 (2024) 110276

Contents lists available at ScienceDirect

Optics and Laser Technology

journal homepage: www.elsevier.com/locate/optlastec

Full length article

Nanowire integration in silica based integrated optical circuits: Limitations and challenges towards quantum computing

Konstantinos Tsimvrakidis [a], Symeon I. Tsintzos [a,1], James C. Gates [b], Peter G.R. Smith [b], Ali W. Elshaari [c], Val Zwiller [c], Christos Riziotis [a,d,*]

[a] Theoretical & Physical Chemistry Institute, National Hellenic Research Foundation, 11635 Athens, Greece
[b] Optoelectronics Research Centre, University of Southampton, SO17 1BJ Southampton, United Kingdom
[c] Department of Applied Physics, Royal Institute of Technology (KTH), 106 91 Stockholm, Sweden
[d] Institute for Advanced Modelling and Simulation, University of Nicosia, CY-2417 Nicosia, Cyprus

ARTICLE INFO

Keywords:
Nanowires
Quantum dot
Waveguides
Silica
Integrated optical circuits
Quantum photonics
Quantum computing

ABSTRACT

Optical integrated circuits suggest a very promising platform for the development of robust and efficient quantum computers. A critical issue to their development and scalability is the integration of multiple single photon sources in the circuits. One major category of single photon sources is based on quantum dots that are embedded in semiconductor optical nanowires (NWQD) that allow their accurate handing and deterministic integration. Successful integrations of such nanowires have been reported in high index platforms like silicon or silicon nitride, with adequate coupling efficiency due the modal characteristics compatibility. On the other hand, Silica-on-Silicon is a major integration platform, which combined with new fabrication approaches like direct laser writing, for the definition of optical structures with refractive index modification, can provide the fabrication of highly optimized and tailor-made circuits by rapid prototyping. Considering for the first time the integration scenario of NWQD in laser written silica-based waveguides it is shown that the low ($\sim 10^{-3}$) achievable refractive index contrast imposes strict limitations on the compatibility of such waveguides with NWQD resulting in general in low coupling efficiency. By considering several design and fabrication issues, suitable integration approaches with adequate efficiency are demonstrated, while also the limitations and challenges are revealed thus triggering new research directions.

1. Introduction

Integrated optical circuits provide a convenient platform for the fabrication of optical based components and devices in a single chip, offering miniaturization, scalability, and loss and phase stability. It is anticipated that they will play a key role in the advancement of quantum photonics, supporting the development of linear optics quantum computers (LOQC) [1], quantum sensing, and quantum communication systems. By enabling on-chip manipulation of the quantum states of light, Quantum Photonic Integrated Circuits (QPICs) [2] have the potential to revolutionize the field. However, there are still significant challenges that need to be overcome, such as the lack of scalability [3,4] by the limitation of the number of single photon sources and the overall number of operating qubits. To develop scalable quantum circuits, it is necessary to have multiple inputs of single photons, which currently is facilitated mostly by photon generation through the inefficient and probabilistic process of parametric down conversion in nonlinear optical waveguides [5]. Integrating single photon sources on a chip is essential for the development of scalable quantum circuits [3,6]. Semiconductor quantum dots (QDs) have been incorporated into QPIC chips to act as single photon and entangled photon generation sources. QD-based single photon sources offer on-demand single photon generation and the advantage of on-chip electrical excitation and wavelength tunable entangled photon emission [7–13]. However, integrating QDs into quantum photonic circuits in a deterministic way is challenging due to their small nanometer-sized dimensions.

By integrating QDs into photonic nanowires (NWs), the emission of the QD can be coupled to the NW's waveguide fundamental mode, resulting in a narrow emission linewidth of Gaussian profile and accurate tunability [11–13]. This makes the NWQD an attractive candidate

* Corresponding author at: National Hellenic Research Foundation, Theoretical & Physical Chemistry Institute, 11635 Athens, Greece.
E-mail address: Riziotis@eie.gr (C. Riziotis).
[1] Present address: QUBITECH Quantum Technologies, 15231 Chalandri, Athens, Greece.

https://doi.org/10.1016/j.optlastec.2023.110276
Received 25 June 2023; Received in revised form 13 October 2023; Accepted 26 October 2023
Available online 2 November 2023

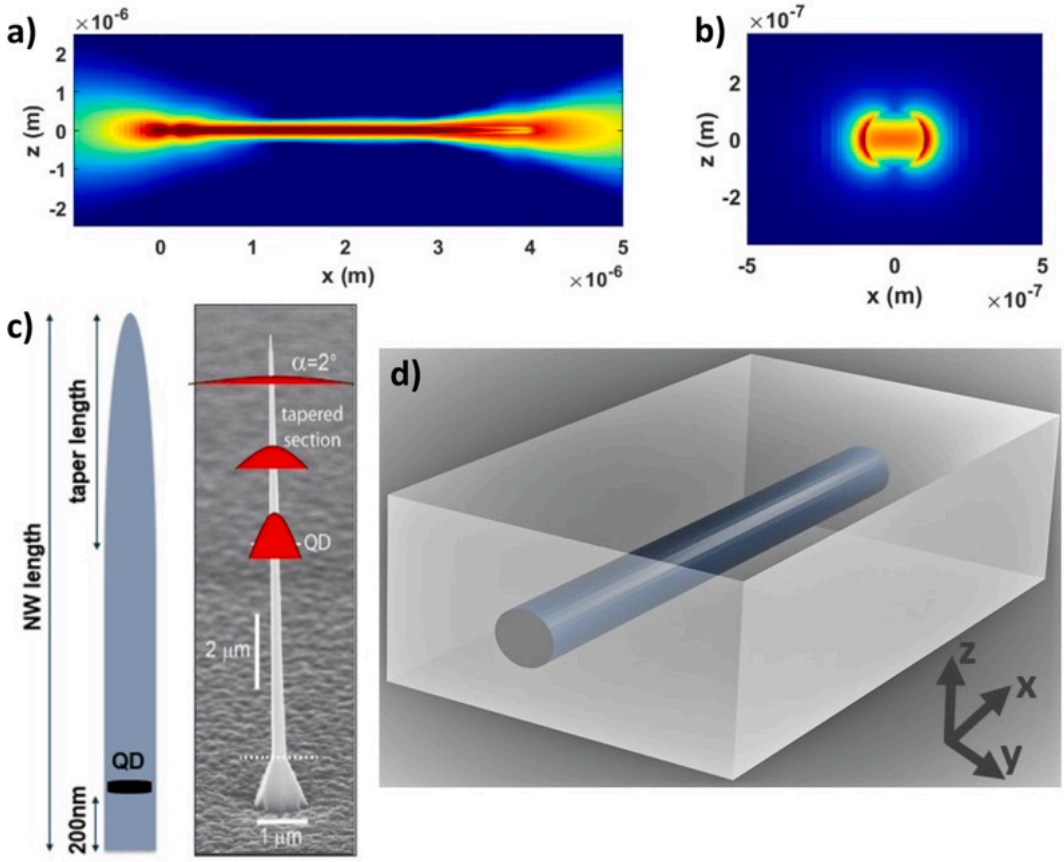

Fig. 1. a) The electric field distribution of an emitting tapered NWQD. b) Nanowire's fundamental TE mode. c) Schematic and SEM image of tapered NWQD (modified from[23]). d) Cylindrical waveguide in a uniform medium.

for specific types of QPICs by enabling further coupling to internal or external waveguiding components [14]. Furthermore, NWQDs can be deterministically embedded in photonic circuits, as their length is in the order of a few to several micrometers and can be manipulated using standard micromanipulation techniques [15–17]. However, direct integration of NWQDs has only been demonstrated in silicon and silicon nitride integrated platforms, due to the compatibility of the waveguide dimensions and refractive indices with the NWQD. This results in high mode overlap and efficient optical power coupling, which is essential for achieving practical quantum photonic devices [14,17,18].

This compatibility allows the efficient coupling to a degree of >20% which is adequate for practical implementations. However, the use of semiconductor integrated circuits poses a challenge for the efficient coupling with silica-based optical fibers due to their different optical characteristics. This incompatibility leads to high insertion losses, which can negatively impact practical applications. Furthermore, the manufacturing process of these circuits using Electron Beam Lithography and Reactive Ion Etching imposes strict limitations on the flexibility of their fabrication.

The integration of NWQDs into silica-based waveguides [5,19] has not yet been studied and explored, possibly due to the differences in material and optical properties and waveguiding behavior between semiconductor optical nanowires and silica-based waveguides. Among others, one of silica platform's advantage is the ability of fabricating silica based optical circuits by Direct Laser Writing - DLW methods [20,21], where the laser induced refractive index modification on silica defines channel waveguides, and offers rapid customization capabilities for the fabrication of complex and highly functional optical circuits. However, this DLW method creates optical waveguides of low refractive index contrast, with typical refractive index increase $\Delta n \sim 5{\cdot}10^{-3}$, with low or medium optical confinement and typical waveguide mode diameter larger than 5 μm setting additional incompatibility and restrictive issues for NWQD coupling to laser written waveguides (or in general to other buried in-diffused waveguides).

This paper investigates for the first time the limitations and challenges for integrating NWQDs in optical waveguides and especially into laser written silica-based circuits [22] which is important for the development of highly customized and optimally designed scalable optical circuits for quantum computing. By identifying limiting issues, the trigger of research for new light coupling architectures is anticipated.

2. Materials & Methods: NWQD-Waveguide coupling system

In this section, it is considered the generic case under study consisting of various types of optical nanowires and generic cylindrical shaped waveguides assumed in the silica material platform system. Buried waveguide structures in homogeneous silica cladding is assumed relating this study to directly inscribed waveguides. Typical fabrication approaches could be direct laser writing by a variety of laser sources from ultraviolet to infrared wavelengths. The corresponding modal characteristics are studied for drawing useful conclusions regarding the modal compatibility of NWQDs and such waveguides. For the purpose of a more generalized study and despite the fact that the material platform considered here is silica, a wide range of refractive index change and waveguide diameter are considered below in order to illustrate the limitations in a more generic view. The study in the current and following sections has been performed by Finite Difference Time Domain (FDTD) simulations.

2.1. NWQD design and optical properties

The NWQD in the following theoretical studies is designed as a

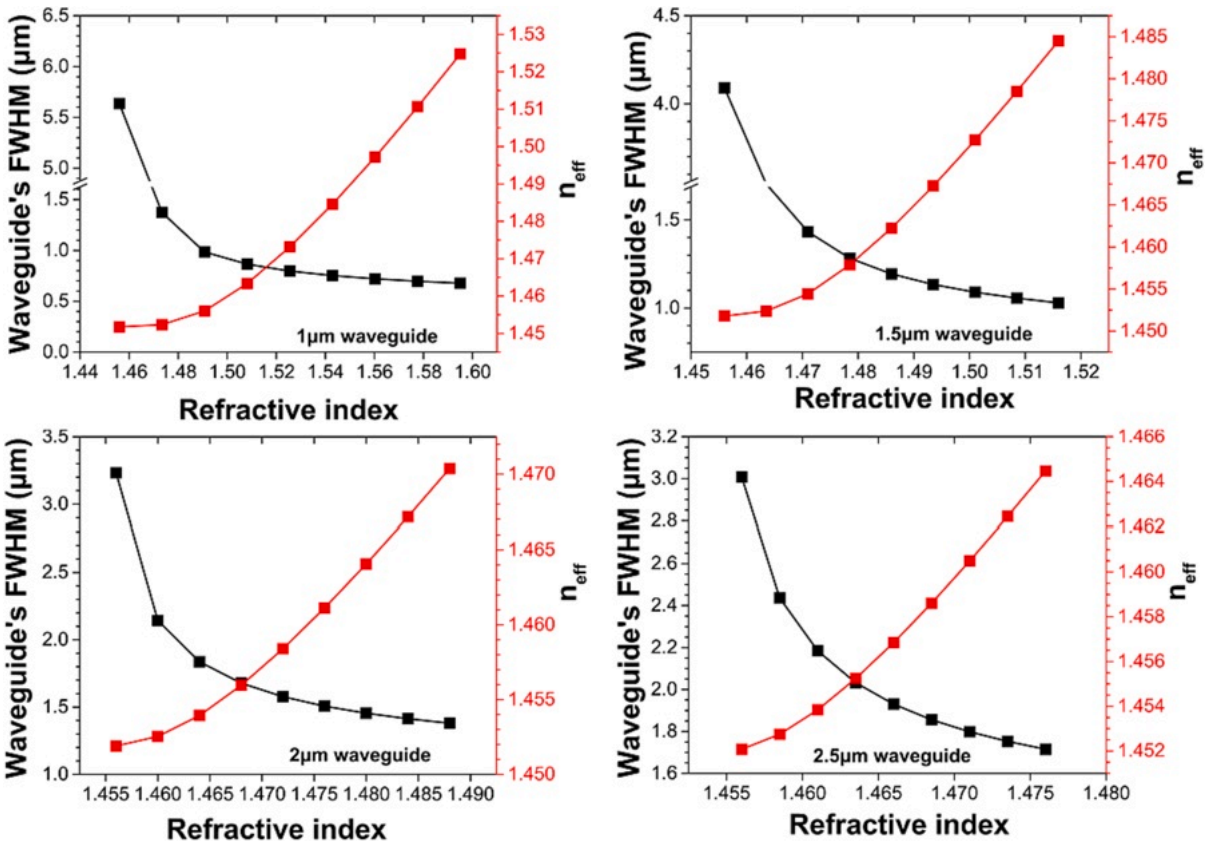

Fig. 2. FWHM and effective index n_{eff} of the waveguides' fundamental TE modes, as a function of the core refractive index for specific waveguide's diameters.

typical state-of-the-art nanowire with a III-V Indium Arsenide Phosphide (InAsP) quantum dot in an Indium Phosphide (InP) nanowire housing. The nanowire is tapered down into a conical structure with the tip diameter being smaller than the base diameter. The tapering assists in minimizing the reflections of incoming light due to the adiabatic increase in the effective refractive index, and in the directionality of the emitted light enhancing the efficiency of coupling into the adjacent photonic component (waveguide). The electric field distribution of a tapered NWQD's emission is shown in Fig. 1. The emission of the nanowire after the tapered end-tip has a Gaussian profile that diverges as a function of the propagation distance. In total four nanowires were designed and considered in the simulations with a constant base diameter of 200 nm. Two of designed nanowires are at a 4 μm length with 1° and 2° tapering angle leading to 109 nm and 154 nm tip diameter, respectively, and the other two are 5 μm long also with 1° and 2° tapering angle leading to 88 nm and 144 nm tip diameter, respectively. Non-tapered nanowires exhibit abrupt radiated field at the end-face of nanowire that increases losses and degrade the coupling efficiency. The quantum dot is simulated by integrating an electric dipole source positioned 200 nm away from the un-tapered end of the nanowire. All the nanowire geometries are designed and tuned for a center wavelength emission at 880 nm. Although this wavelength was selected as such NWQD are the most common option with high availability for experimental verification, the specific characteristics considered in the study do not restrict the applicability of the results in other operating wavelength bands.

2.2. Generic form of cylindrical optical waveguides

The considered waveguides are of cylindrical shape with circular cross-section profile (Fig. 1d), simulating laser written channel waveguides. The medium in which the waveguide lays in a uniform material with refractive index n = 1.452 (considered at 880 nm operating wavelength) to mimic a standard silica material system. Various waveguide sizes are designed from 1 μm to 2.5 μm diameter with a step of 0.5 μm. In laser written silica channel waveguides, a typical refractive index change (Δn) due to laser induced modification is in the order of $\Delta n = 5{\cdot}10^{-3}$. However, in order to fully understand how the waveguide behaves in terms of its core refractive index, the modification span examined is much wider. Therefore, the refractive index of the waveguides is set to a range from n = 1.456 up to a value where each waveguide remains single mode just before exhibiting a second TE mode. Fig. 2, shows the full width at half maximum (FWHM) and the effective index n_{eff} of each waveguide fundamental mode for the range of refractive index values in which they retain the single mode operation.

2.3. Comparison of the modal characteristics of NWQD and waveguides

To achieve optimal coupling between the NWQD and the waveguide, it is rational to assume that the spatial modal extent of the NWQD emission should match the spatial extent of the waveguide mode as closely as possible. This means that the FWHM of the NWQD emission spectrum should be as close as possible to the FWHM of the waveguide. If the FWHM of the NWQD emission is too large compared to that of the waveguide, then the overlap integral between NWQD emission and the waveguide modal fields will be reduced, leading to lower coupling efficiency. Conversely, if the FWHM of the NWQD emission is too small compared to the FWHM of the waveguide, then only a fraction of the NWQD emission will be coupled into the waveguide mode, again resulting in lower coupling efficiency.

In the case that the FWHM of the NWQD emission spectrum does not match the mode field diameter of the waveguide, increasing the distance between the NWQD and the waveguide can help to improve the coupling efficiency. By increasing the distance between the NWQD and the waveguide, the overlap integral between the NWQD emission and the

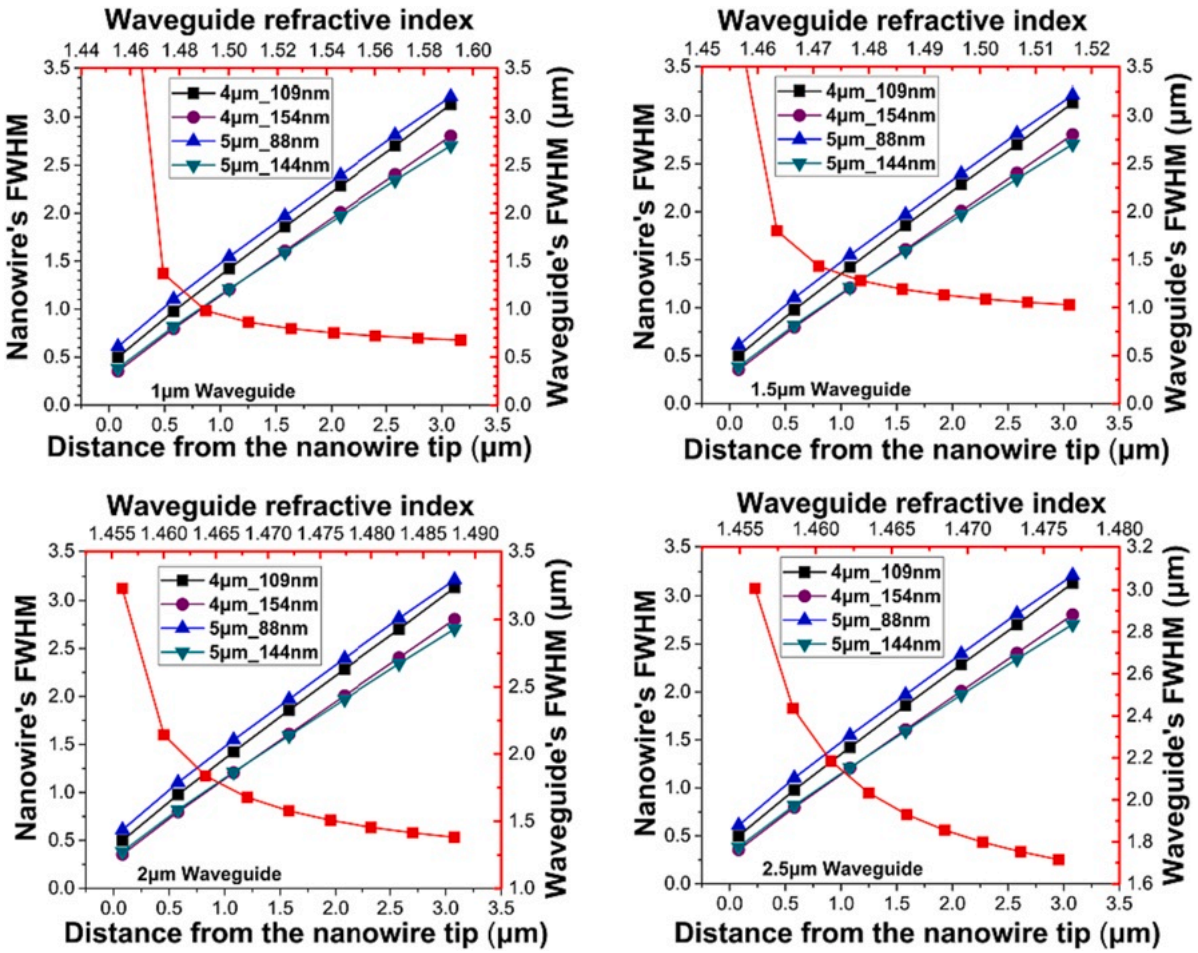

Fig. 3. Comparison between the FWHM of the NWQD emission at various distances after the tip end and the FWHM of 1, 1.5, 2 and 2.5 μm diameter waveguides versus their refractive index (marked as red).

waveguide mode could be improved, as the NWQD emission will have a larger spatial extent and a higher overlap with the waveguide mode. However, increasing the distance could also lead to increase of free space radiation losses from NWQD, which can ultimately, under this competitive process, result in a lower overall coupling efficiency.

In Fig. 3, the FWHM of the NWQD emission is shown for each nanowire geometry at the tip's end and after a few micrometers and is compared to the FWHM of each one of the designed waveguide diameters for a range of core refractive index values. Ideally, the FWHM of a given waveguide with a specific refractive index value should be matched to the FWHM of a NWQD emission and set the appropriate distance between the components. It can be observed that for increased waveguide dimension it is required a high refractive index difference and an increased distance between NWQD and waveguide. However, the increased distance results in increased losses and act competitively to the mode matching succeeded. This simplified approach provides some intuitive indications of the NWQD and waveguide mismatch and suggests that the problem needs more radical handling like true coupling calculations through FDTD numerical simulation as will be presented below.

3. NWQD coupling in cylindrical waveguides

The different geometrical and optical characteristics of the waveguide and NWQD result in different numerical apertures and guided mode FWHM and consequently to different modes' overlap and energy transfer. Tapered NWQDs, as considered here, emit a Gaussian beam but still the incompatibility of NWQD emitted beam limits the coupling. Since the modal characteristics depend only on the optical and geometrical characteristics of the nanowire and define the coupling mechanism, in the following analysis it is considered only the guided mode of the nanowire while the effect of the embedded QD is neglected for simplicity in the simulations presented. This simplified consideration results in a linear constant difference between the estimated coupling of light between the case of nanowire and waveguide, and the case NWQD and waveguide, which is attributed to the coupling ration of the QD in to the nanowire. This coupling ratio has been calculated and is ~ 67% for the studied cases, resulting thus in a corresponding overestimation of coupling by simply employing nanowires.

3.1. Inline arrangement

In the inline arrangement scenario, there is a silica medium (n = 1.452) in which the nanowire is either butt-coupled / end-firing the waveguide with some distance L between them, as shown in Fig. 4a. Performing FDTD simulations, the coupling efficiency values are extracted for all four designed nanowire geometries and for each waveguide diameter, assuming they are in contact at L = 0 μm. While the nanowire geometry seems to affect the overall coupling efficiency, this is evident mostly for waveguides of higher confinement with high refractive index values. The core refractive index appears to be the dominant parameter playing a major role in the coupling of the emitted light, starting from down to almost 0% for weak refractive index modification up to about 70% for narrow waveguides with $\Delta n = 1.5 \cdot 10^{-1}$. The waveguide diameter defines also the range of coupling as for very spatially confined waveguides (1 μm diameter) which is closer to NWQD

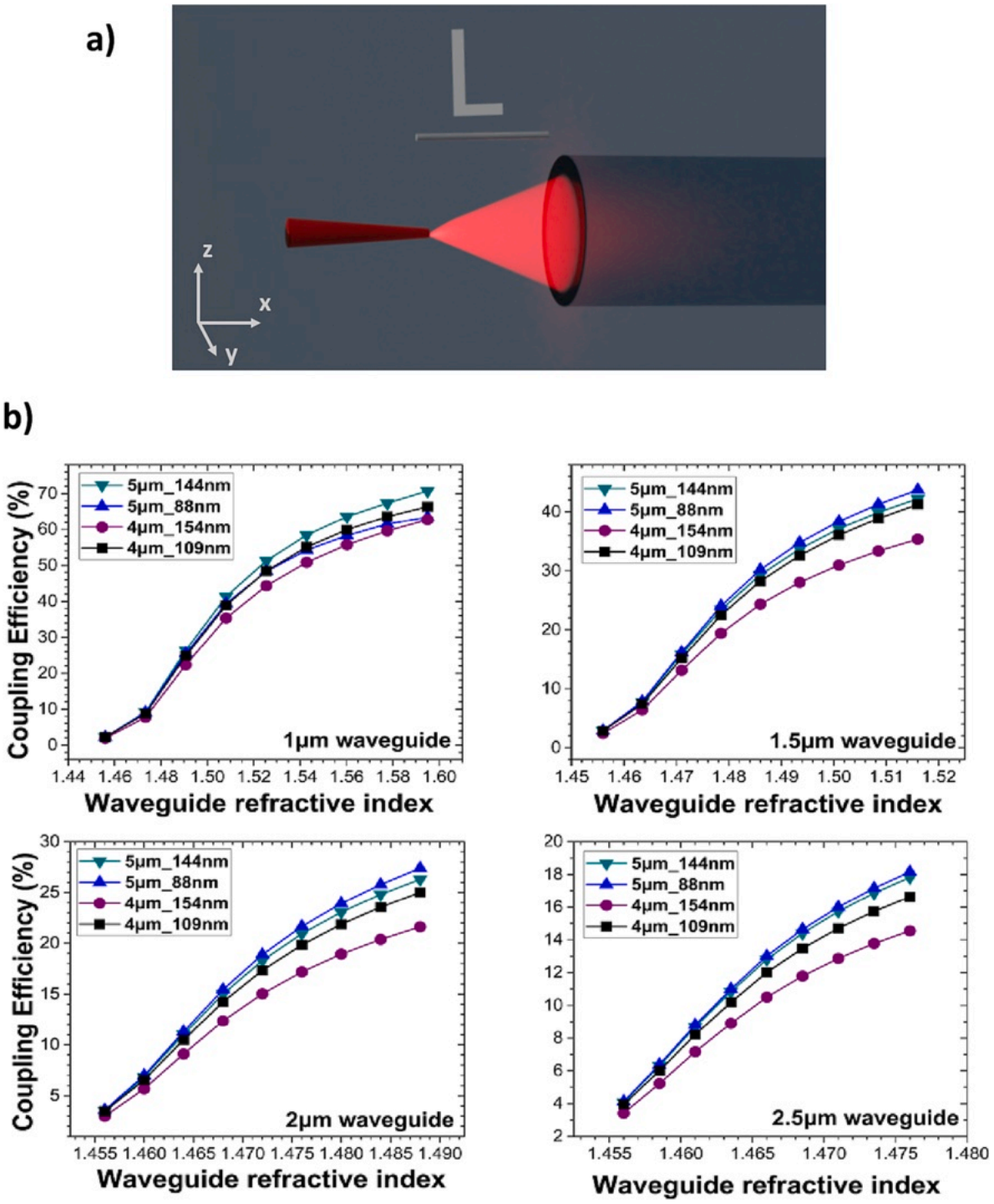

Fig. 4. a) Schematic illustration of the inline arrangement. b) Coupling efficiency extracted in the inline arrangement for each nanowire and waveguide geometry.

geometrical characteristics the coupling is much higher.

3.1.1. *Effect of distance*

Additionally, the effect of increasing the distance L between the nanowire and the waveguide is examined for L = 1 μm, 1.5 μm, 2 μm and, 2.5 μm. In Fig. 5a, the coupling efficiency values of all four waveguides are presented, maintaining the same refractive index value span, for distance L up to 2.5 μm. Calculations were performed after propagation at 100 μm, where the confinement of the coupled light in the waveguide has been stabilized from transient phenomena, as seen in Fig. 5b. For clarity, in the presented graphs only one nanowire geometry is considered, at 4 μm length and 109 nm tip diameter. The rest of the nanowire geometries, while not shown here, are found to follow the same trends. At an increasing distance, as expected the effects are more evident for higher refractive index waveguide values. It is observed that for the narrower waveguides with diameter 1 μm or 1.5 μm, butt coupling the nanowire leads to higher coupling efficiency values, while for the larger ones with diameter 2 μm and 2.5 μm, introducing some intermediate distance between them leads to slightly better coupling, even for waveguides of lower refractive index.

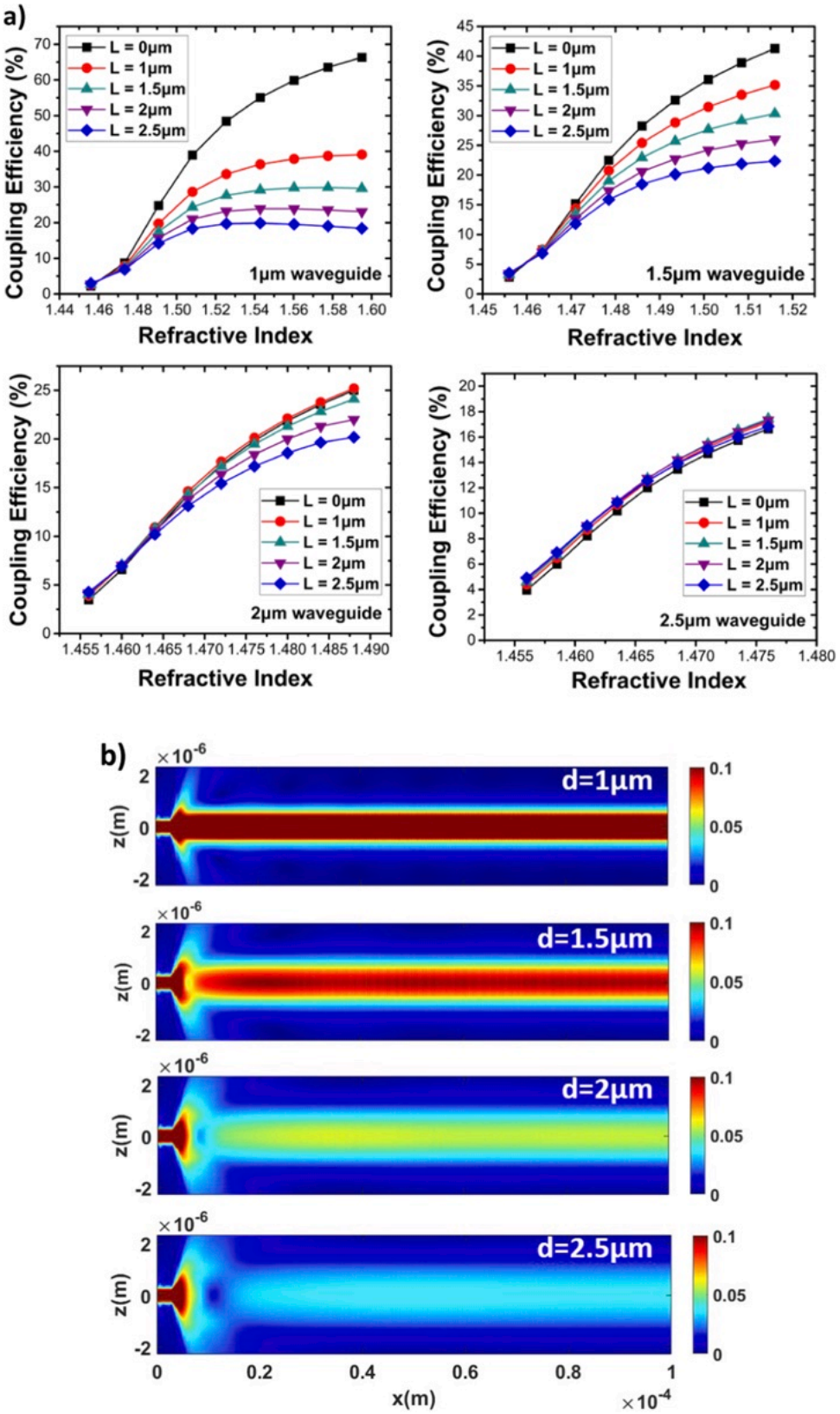

Fig. 5. a) Coupling efficiency over waveguide's refractive index for various nanowire-waveguide distances L. b) The electric field distribution along the propagation axis X (for distance 100 μm) for the corresponding highest refractive index waveguides at L = 0 μm with diameter from d = 1 μm to d = 2.5 μm .

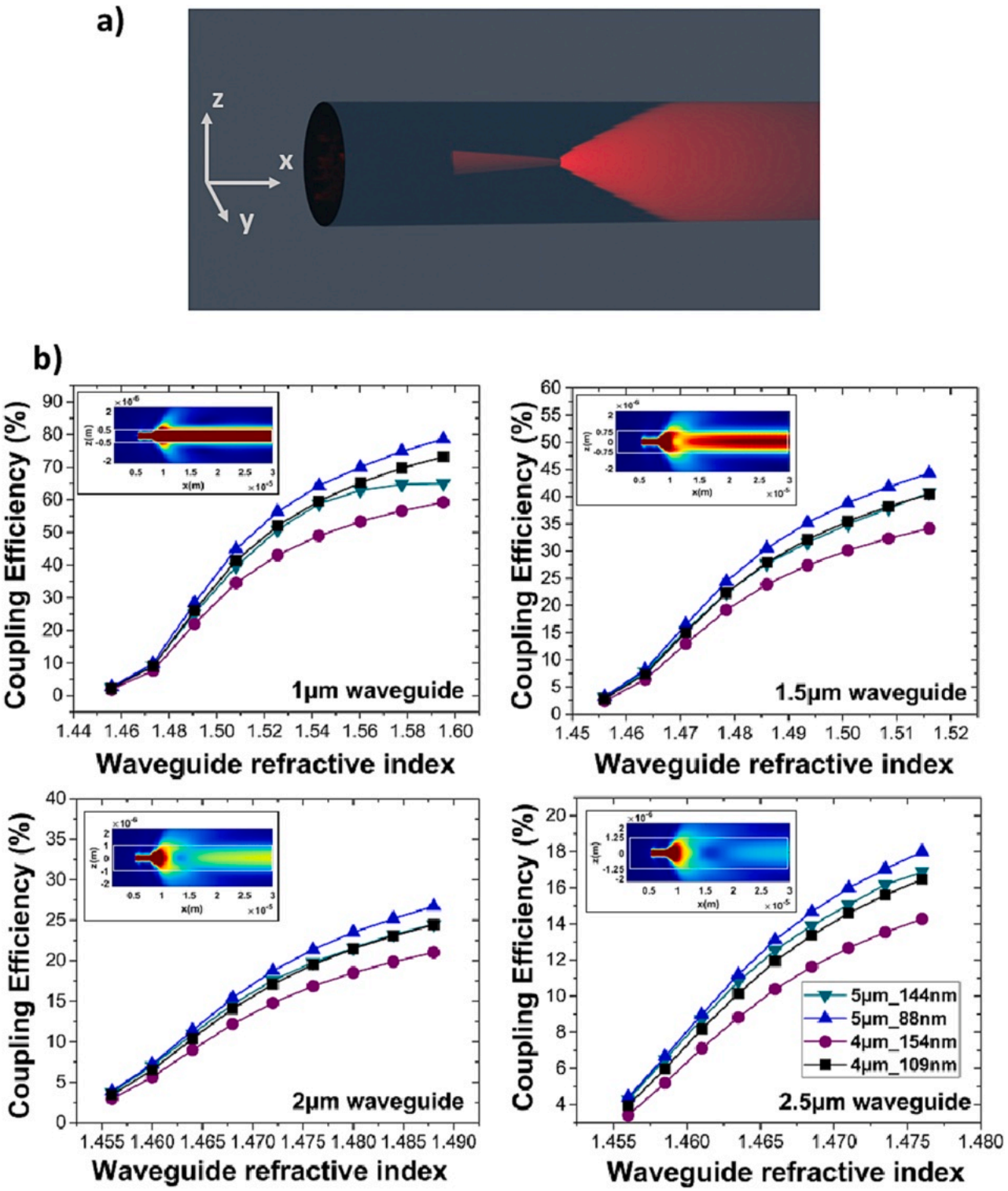

Fig. 6. a) Illustration of the embedded arrangement. b) Coupling efficiency extracted in the embedded arrangement for each nanowire and waveguide geometry. Inset images show the electric field distribution along the propagation axis for the 4μm_109nm nanowire at the highest refractive index waveguides for the propagation distance of 30 μm.

3.2. Embedded arrangement

Here, the nanowire is designed to be embedded, in a theoretical approach not directly physically realizable, positioned inside the waveguide, as shown in Fig. 6a, intended to provide a comparison to the aforementioned inline arrangement. In contrast to the previous arrangement where the nanowire is in line to the waveguide, in the embedded arrangement the nanowire being inside the waveguide aims for an enhancement of mode overlap and coupling. However, as seen in Fig. 6, the coupling efficiency values extracted from all nanowire-waveguide combinations do not differentiate much from those of the inline arrangement. Similar trends are observed, with the nanowires' geometry and the waveguide diameter combinations resulting in slightly higher coupling efficiency values, at the given refractive index value

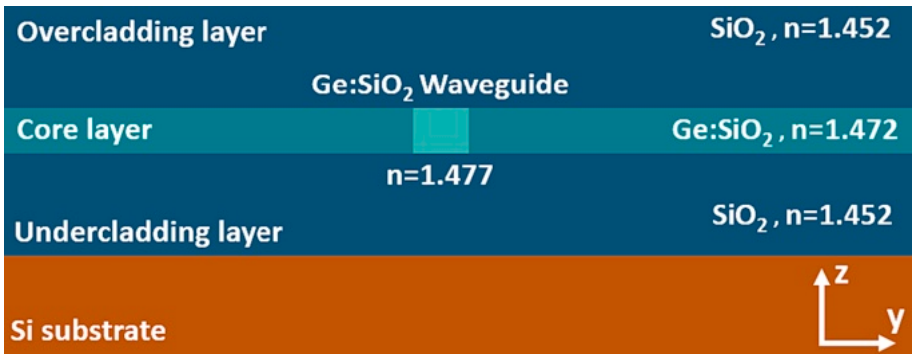

Fig. 7. Illustration of the 3-layer silica-on-silicon device (Y-Z cross section).

span.

Despite achieving theoretically high coupling efficiency values for the ideal case of cylindrical waveguides this occurs only for waveguides with high refractive index difference and with confined waveguide geometry for diameters < 2 μm. It is obvious that there are major limitations to their practical implementation, first on the size of waveguides and second on the refractive index contrast. The cylindrical waveguides examined could simulate femtosecond laser written waveguides that typically exhibit Δn values equal to about $5{\cdot}10^{-3}$ [24,25]. Such refractive index values are not sufficient for efficient light confinement and as shown in both arrangements the outcome performance lays in the order of 2–4% of coupling efficiency.

This work is motivated by waveguide circuitry made by direct laser writing, by either femtosecond or ultraviolet continuous wave (CW) sources. Current fabrication capabilities do not allow implementation of such highly confined waveguides. Even if such narrow width and high refractive index contrast waveguides could be fabricated the resulted mode profile would be much narrower than the standard mode profile in such circuits that are intended to match the single mode fiber (SMF) characteristics for low insertion loss. Alternative approaches such as adiabatic index or diameters tapering, could be used but with the cost of additional circuitry and fabrication complexity.

4. Coupling performance in silica-on-silicon platform

The silica-on-silicon platform is a well-known and established integrated photonics platform, which provides considerable design flexibility by tailoring the properties of the layers by selective doping in order to adjust the layers' refractive indices and the core layer photosensitivity. As a mechanically robust platform it provides also means of fiber connectorization with long term stability. Selective Ge-doping of core layer can adjust refractive index of the core layer and provide additional degrees of freedom compared to uniform silica substrate.

Here, a silica-on-silicon platform was designed and combined with a suitably embedded NWQD. The system follows a 3-Layer configuration where the undercladding and overcladding layer is a silica layer (n = 1.452) and the core layer is of a higher refractive index material. Usually, such core layers are achieved by doping the standard silica with germanium ($Ge:SiO_2$), leading to a much higher refractive index photosensitive layer. Depending on the doping level of germanium in the core silica layer (0.66% to 2%) the refractive index change of the core layer can be up to $\Delta n = 2{\cdot}10^{-2}$. Such platforms are used widely for the definition of optical circuits by using ultraviolet laser in DLW techniques [20]. On the core layer a channel waveguide can be accurately fabricated (with DLW/UV-writing technique) and apply an additional $5{\cdot}10^{-3}$ refractive index change on the laser induced channel waveguide. With a base silica refractive index value n = 1.452, the formed waveguide can end up in a value of n = 1.477, with horizontal $\Delta n = 5{\cdot}10^{-3}$ and vertical $\Delta n = 2.5{\cdot}10^{-2}$ index contrast, as can be seen in Fig. 7. The resulted single mode waveguide is considered of rectangular shape and

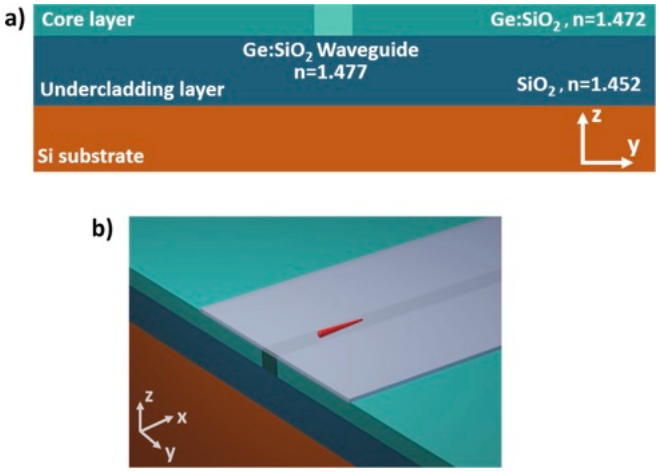

Fig. 8. a) Schematic of the 2-Layer profile and b) Artistic representation of the NWQD on top of the chip.

lateral dimensions 3 μm × 3 μm, which is experimentally achievable. This flexibility provided by the 3-layer platform and UV direct writing could allow for enhancement of coupling overcoming the aforementioned limitations.

4.1. On-top placement for evanescent coupling

The easiest way to access the waveguide and to place the NWQD is by an on-top placement, facilitating an evanescent coupling between the two components. This approach has been extensively used in coupling of nanowires in silicon, or silicon nitride waveguides providing efficient coupling [14,17,18]. Therefore, for demonstrating the differences of high index platforms with silica-based platform, this approach is also considered here, where the NWQD is designed to rest on top of the waveguide for evanescence coupling to the waveguide. It is assumed that the silica overlayer above the channel waveguide is removed, or the entire optical chip is based on a 2-Layer configuration with no overcladding silica layer as seen in Fig. 8. This configuration allows for easy access and manipulation of the NWQD leading to an easier integration. Also, it gives the flexibility to include high index layers to serve as intermediates for efficient coupling. Thus, a new 3-layer structure is achieved by depositing a thin dielectric layer (n = 2.1) as the overcladding layer on top of the core layer. The addition of the dielectric layer will assist in "lifting" the waveguide's TE mode field and better couple with the NWQD emission by improving their overlap.

Two indicative studies are presented to demonstrate the limitations of this scheme, one with a waveguide 1.5 μm × 1.5 μm and one with 3 μm × 3 μm, both at n = 1.477, as presented in Fig. 9 and Fig. 10 respectively. Fig. 9a and 10a present fundamental TE mode profiles for a

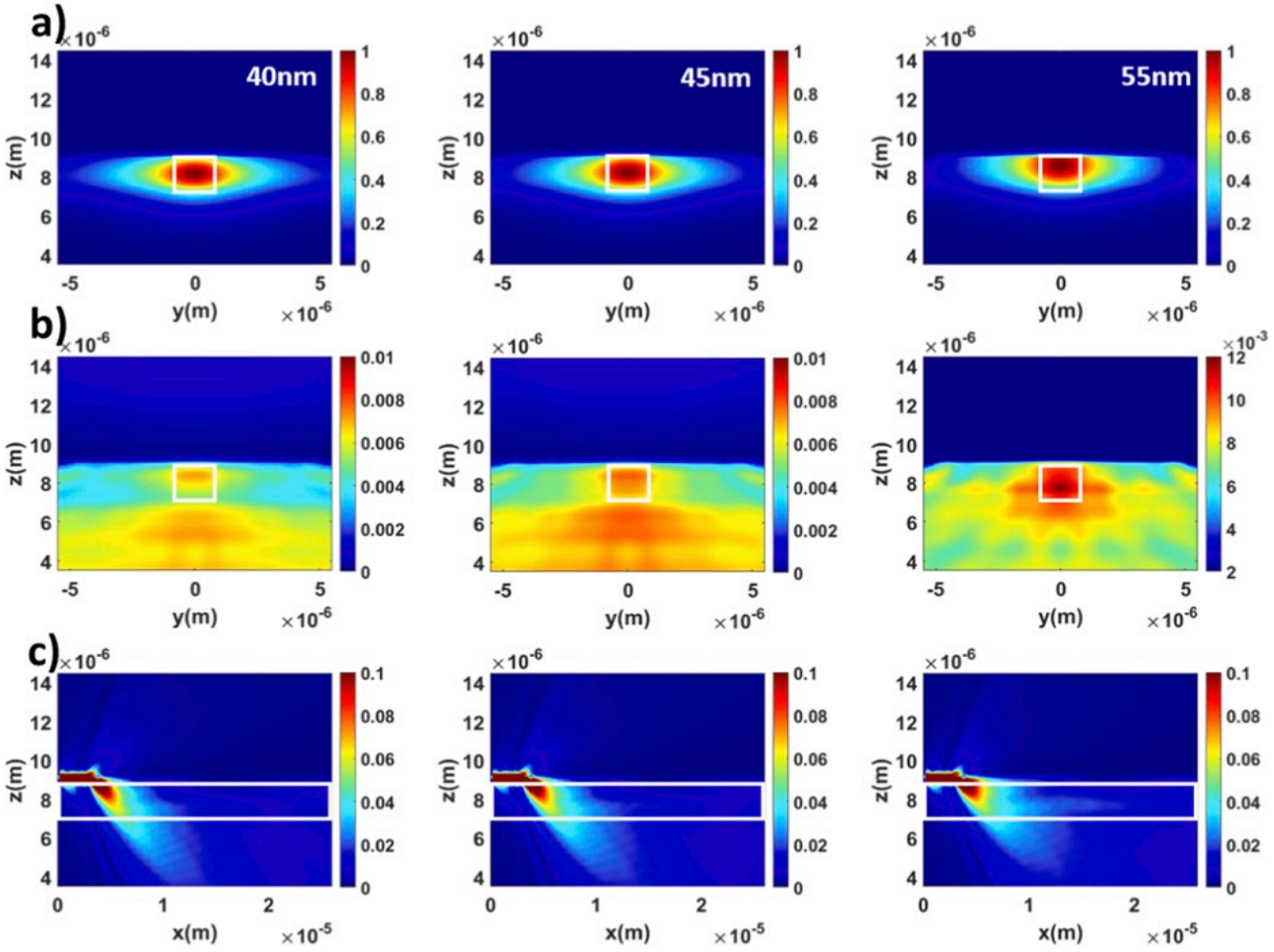

Fig. 9. Coupling between nanowire and waveguide for various thicknesses of high index over-layer. a) Waveguides fundamental TE mode profile for a channel waveguide of 1.5 μm × 1.5 μm cross section dimensions, b) Field distribution at the end of propagation at 25 μm and, c) Corresponding electric field distribution along the propagation axis, over different overcladding layer thicknesses for propagating distance of 25 μm.

specific channel waveguide of (1.5 μm × 1.5 μm, or 3 μm × 3 μm). The second rows (Fig. 9b and 10b) present the field distribution at the end of propagation at 25 μm where is obvious that the concentration of field is higher for the narrower waveguide. The third rows (Fig. 9c and 10c) present the corresponding electric field distribution along the propagation axis where it can be noticed the low confinement in the optical waveguide. Depending on the dielectric layer thickness (35–65 nm) the coupling process changes and becomes more efficient for higher thickness, however in all cases the coupling is highly inefficient as the emitted light by NWQD drastically escapes and diffuses into the surrounding undercladding.

While testing only one NWQD geometry, a longer nanowire with a longer tapering region would increase the interaction area between the nanowire and the waveguide and would potentially be able to transfer more energy into the system. However, by testing this case also the coupling was still low and impractical (not shown here). A possible solution would be to embed a reflective layer between the core layer and undercladding but this would greatly increase the complexity of the structure. It is obvious by the presented results that the on-top approach cannot provide efficient coupling solutions and other approaches need to be investigated and devised.

4.2. Inline arrangement

Alternatively, as an obvious arrangement case, the NWQD is positioned inline aligned to the waveguide for end-firing coupling arrangement. The NWQD needs to be placed in the middle of the core layer thickness in a suitable physical hosting slot, and aligned with the channel waveguide for end-fire coupling as shown in Fig. 11a. The access to the buried waveguide and the pattering of a suitable physical slot/trench is possible by femtosecond laser ablation and micromachining [24,25] or by Focused Ion Beam (FIB) milling or Reactive Ion Etching (RIE), depending on the depth of the required features. To achieve a perfect alignment of the nanowire axis to the center of the channel waveguide, a high degree of control of the depth of the fabricated slot is required, however current techniques like RIE and FIB can easily provide such accuracy in the order on a few tens of nanometers. The accurate placement and alignment of the NWQD to the slot aligned to the waveguide is also possible by “pick and place” techniques [16,17] with nano/micro-manipulators with typical axial resolution 30 nm and angle of 1°. The micro-machined slot for NWQD hosting could then be covered by suitable polymeric material to match the refractive index of the silica cladding. The overcladding layer considered here is silica, same to the undercladding layer (n = 1.452), the core layer is set to n = 1.472 ($\Delta n = 2{\cdot}10^{-2}$) and the waveguide at n = 1.477 ($\Delta n = 2.5{\cdot}10^{-2}$). Carrying out FDTD simulations with the proposed structure with the NWQD being inline to the waveguide at various distances L, coupling efficiency values of up to 7% are feasible, as shown in Fig. 11b. This denotes a substantial increase in the coupling, taking into consideration the bigger waveguide cross section area (3 μm × 3 μm compared to the

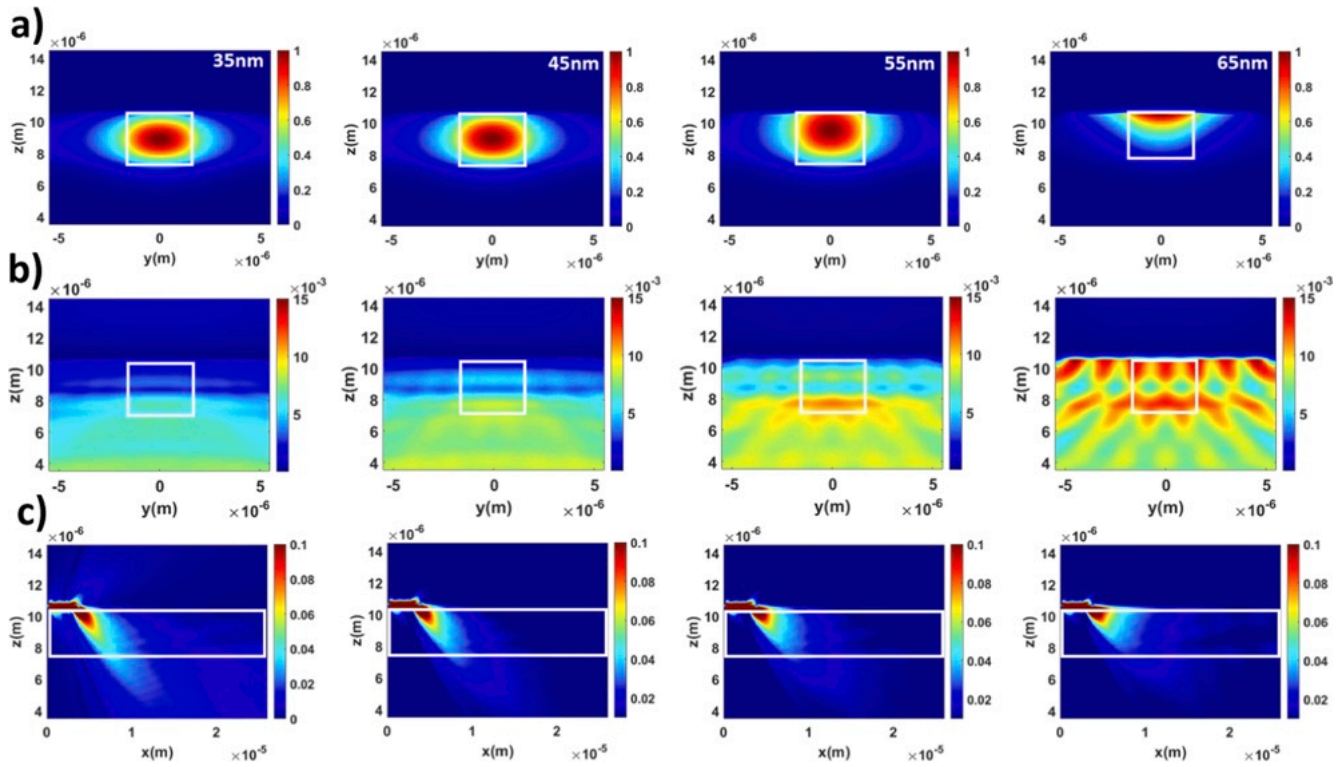

Fig. 10. Coupling between nanowire and waveguide for various thicknesses of high index over-layer a) Waveguides fundamental TE mode profile for a channel waveguide of 3 μm × 3 μm cross section dimensions, b) Field distribution at the end of propagation at 25 μm and, c) Corresponding electric field distribution along the propagation axis, over different overcladding layer thicknesses for propagating distance of 25 μm.

≤ 2.5 μm diameter cylindrical waveguide).

The wave propagation and the coupling efficiency are monitored unidirectionally. However, the quantum dot in the nanowire once excited it emits in both directions as depicted in Fig. 1a. This means that a significant amount of energy is lost by exiting the back end of the nanowire. Therefore, by placing a Bragg grating reflector tuned for the specific NWQD wavelength, or a broadband mirror by depositing a suitable metal layer the backward emitted light can be reflected forward and lead it into the waveguide, as it was proposed in [17]. By the accurate integration of a NWQD in the chip a coupling value well above 10% could be feasible. It was also confirmed that despite the asymmetricity of the channel waveguide the coupling to TM modes retains the same degree of coupling.

4.3. Coupling through a modified ridge waveguide

In an attempt to further investigate the coupling of the NWQD, it was considered the case of a ridge channel waveguide with no overcladding for examining the performance in stronger confined waveguides in silica. This waveguide architecture is relevant to typical silica based circuits made by lithography techniques such as RIE [19] followed by overcladding deposition, or even with no overcladding. In this approach here, a part of the buried channel waveguide was exposed by removing the overlayer and the adjacent parts of core layer in order to reveal the laser written waveguide as a ridge waveguide with a refractive index (n = 1.477). The schematic is illustrated in Fig. 12a.

In this configuration, since the waveguide is exposed to the much lower refractive index of surrounding air (n = 1), the initial 3 μm × 3 μm rectangular waveguide operates in more than one mode. Thus, different waveguide geometries were examined either for single or multi-mode operation at various sizes, while only the indicative cases at 2 μm × 2 μm and 3 μm × 3 μm are presented here because are closer to practical fabrication limits. The supported TE mode profile for a 2 μm × 2 μm and 3 μm × 3 μm ridge waveguide are shown in Fig. 12 b-c. Alternatively, to ensure the single mode operation in the circuit a smaller ridge waveguide could be designed and tapered out into a wider channel waveguide for adiabatic mode transformation [26]. The exposed area could also be covered by a low refractive index material (e.g., a typical encapsulating polymer material like CYTOP with n = 1.34), in order to secure and stabilize in practical implementation the placed nanowire. Such a low refractive index polymer would still maintain a reasonably high index contrast Δn between the ridge waveguide and the surrounding, providing also easier conditions for single mode operation and less drastic width tapering.

An exhaustive number of arrangements of the nanowire with the exposed ridge waveguide were considered by examining various parameters. However, it was concluded that the ridge geometry could not provide any improvement in the coupling but in contrary exhibited worse performance than the much simpler inline arrangements presented above. For complicity, below, are presented some indicative cases and examples.

4.3.1. NWQD on-top of ridge waveguide

In the first case the NWQD rests on top of the ridge waveguide (Fig. 13a) which is exposed to air (n = 1). The light couples evanescently to the ridge waveguide, but due to high refractive index contrast between the surrounding air (n = 1) and the silica undercladding layer, the light diffuses out of the waveguide into the substrate, as shown in Fig. 13b and 13c, for a 2 μm × 2 μm and 3 μm × 3 μm ridge waveguides, operating in single and multi-mode waveguiding conditions respectively.

The light transfer form NWQD follows the same trend in both cases. In the above figures is obvious the interface, positioned at ~ 60 μm, of the ridge and the buried channel waveguide. In the ridge section is observed a high frequency waving, possibly by the coupling process of the NWQD or the reflection by the vertical silica over clad at the beginning of the buried waveguide. In the buried section, after 60 μm, there is a faint light propagation due also to mode mismatching, and

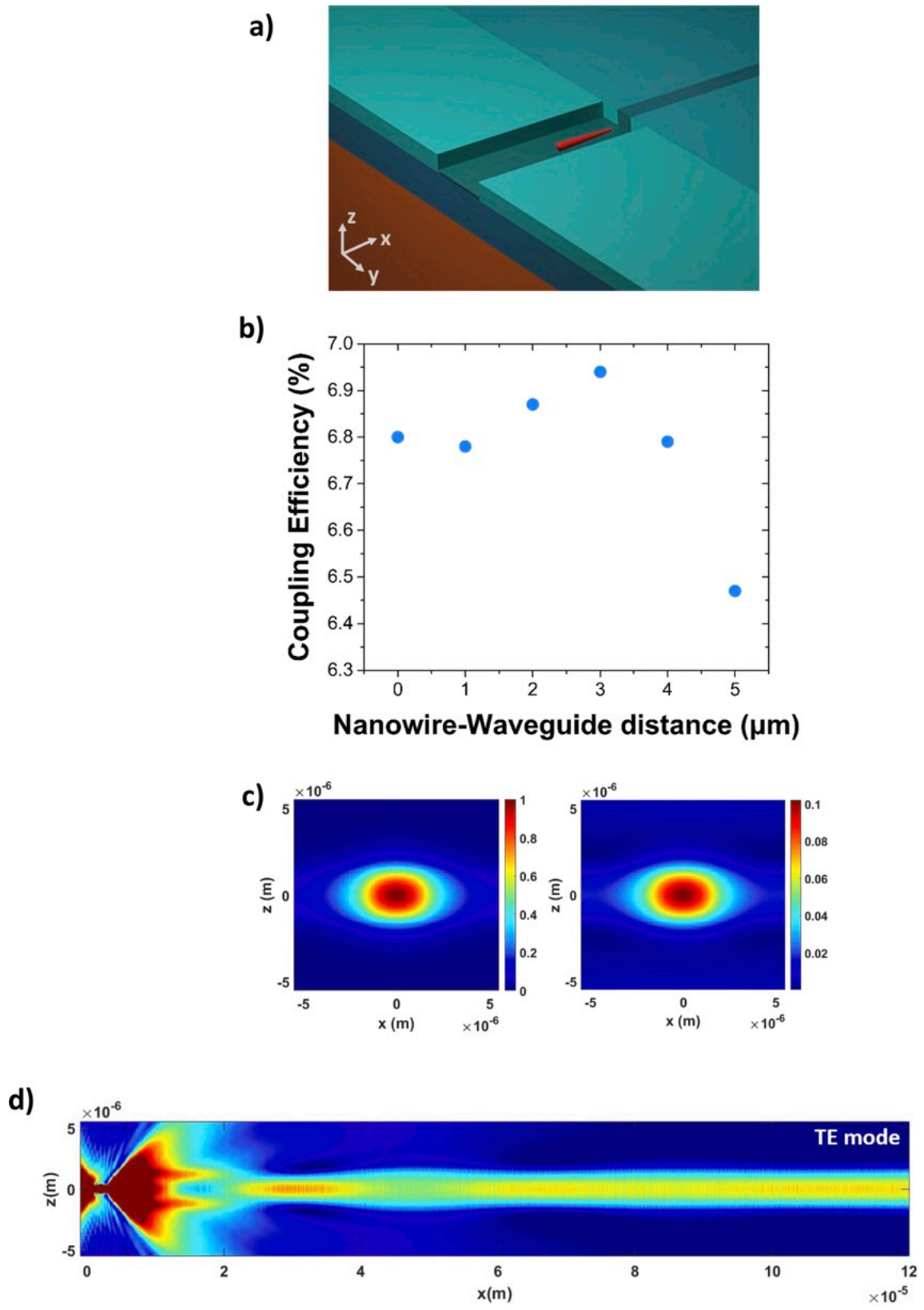

Fig. 11. a) Artistic representation of the NWQD inline to the channel waveguide. b) Coupling efficiency values extracted from the inline arrangement for NWQD-waveguide distance L = 0–5 μm. c) The channel waveguide's supported TE mode (left) and the output profile after 120 μm of waveguide propagation (right). d) The electric field distribution along the propagation axis for 3 μm gap between the NWQD and the waveguide.

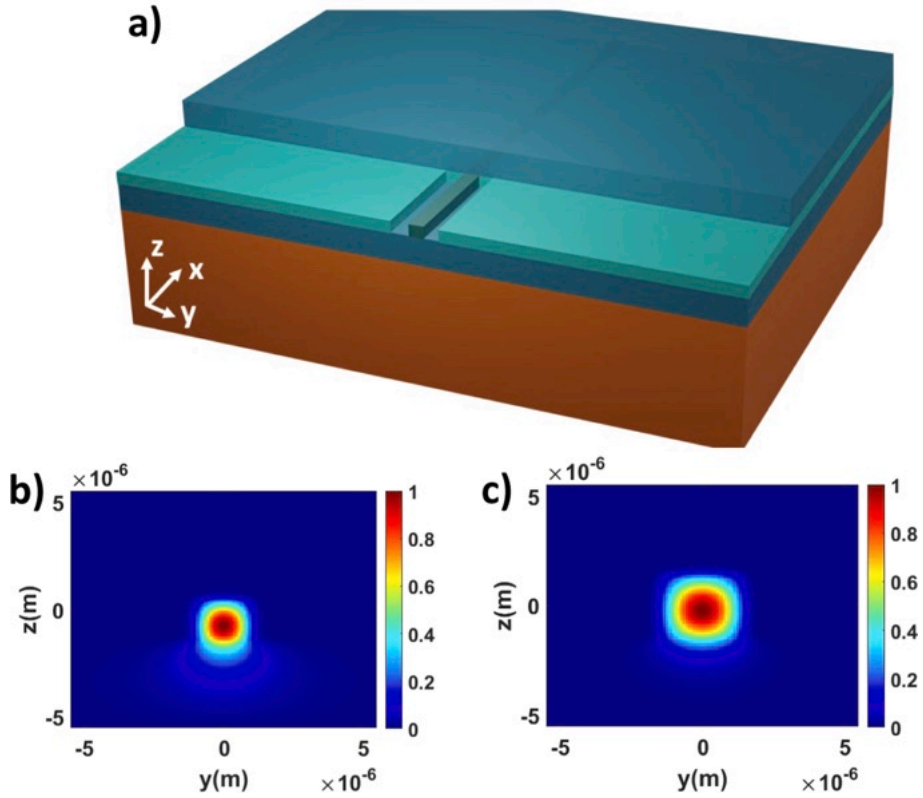

Fig. 12. a) Artistic representation of the exposed ridge waveguide to air. b) TE mode profile of a 2 μm × 2 μm ridge waveguide, and c) TE mode profile of a 3 μm × 3 μm ridge waveguide.

inefficient thus light coupling, between the ridge and buried waveguides.

By considering the lowering of this contrast by the use of a polymer coating (CYTOP, n = 1.34) the radiated light to the undercladding was decreased but still the overall coupling was very low and finally impractical. It is clear that in such an arrangement a number of optimization issues needs to be considered in a thorough study.

4.3.2. NWQD on-top of the ridge waveguide through high index layer

Another modification considered was the introduction of a high index coating on top of the ridge waveguide and the placement of the nanowire afterwards, as can be seen in Fig. 14a. High index overlayers with n = 1.7 to 2.1 and thickness from 50 nm to 100 nm were employed, however there was no improvement in the coupling. Fig. 14b shows an indicative light coupling process for a 50 nm overlayer with n = 2.1, where the light diffusion in the underclad and the parasitic guiding in the overlayer area are apparent limiting thus the coupling to the guided mode.

4.3.3. NWQD end-firing the ridge waveguide

In order to improve the light coupling into the ridge waveguide so it can be transferred into the channel waveguide, an alternative route is followed by placing the NWQD in contact and inline (aligned) to the ridge waveguide. Here, the ridge waveguide is shorter in height by about 1.5 μm at the outer end so that the NWQD is placed on it and points at the center of the rest of the 3 μm × 3 μm ridge waveguide. The NWQD and ridge waveguide is surrounded by air (Fig. 15a). In Fig. 15b can be observed that there is an initial coupling of light into the ridge waveguide which later is lost in its attempt to enter the channel waveguide at the interface positioned at ~ 60 μm. However, in this case as well there is a vast amount of the input light exiting the waveguide during the first micrometers of propagation. The light was also diffused in the material underneath similarly to the on top configuration, as seen in Fig. 13.

4.3.4. NWQD embedded in the ridge waveguide

Finally, it is considered the theoretical arrangement where the NWQD is embedded in a seamless arrangement in the ridge waveguide (Fig. 16), where the coupling between the NWQD emission and the ridge waveguide appears to be more efficient. However, as shown in Fig. 16b, a strong modulation is observed as the light propagates along the 3 μm × 3 μm ridge waveguide and not being able to couple efficiently into the buried channel waveguide that appears in the position of ~ 60 μm along the propagation axis.

The observed beating may be the result of multiple modes propagating inside the 3 μm × 3 μm ridge waveguide, and interface reflections, however consideration of narrower single mode waveguides did not eliminate this beating and did not improve the overall coupling.

5. Conclusions

In summary, the paper presents a theoretical and numerical simulations-based investigation on incorporating a nanowire quantum dot emitter in an integrated photonic circuit, showcasing the challenges and limitations related to achieving efficient coupling between the single photon source and the optical waveguides. A thorough study was presented on the requirements of the coupling between the NWQD and the waveguide, analyzing their optical and geometrical properties. A total of four different NWQDs were examined in relation to a silica-based optical waveguide defined by processes like DLW, revealing the design limitations due to low confinement of the laser-written waveguides. Different NWQD-waveguide configurations were considered in this generic silica platform scenario with cylindrical channel waveguides, namely, a) inline arrangement with the NWQD for end-fire coupling into the waveguide and b) embedded arrangement where the NWQD is hosted inside the waveguide. While, high coupling efficiency values were acquired for high refractive index waveguides and narrow waveguides, these conditions are unrealizable as in a more pragmatic

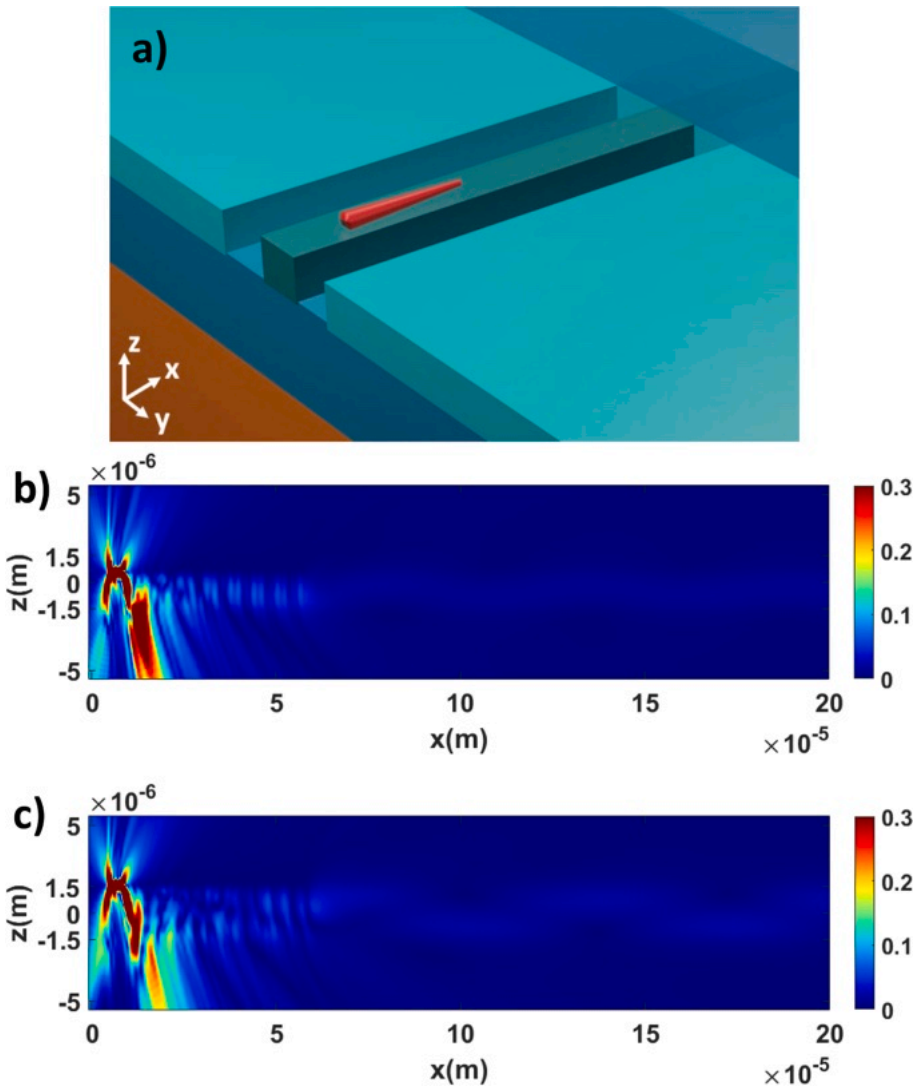

Fig. 13. a) Illustration of the NWQD on top of the ridge waveguide, b) Electric field distribution along the propagation axis of a 2 μm × 2 μm ridge and channel waveguide with the NWQD on top, c) Electric field distribution along the propagation axis of a 3 μm × 3 μm ridge and channel waveguide with NWQD on top.

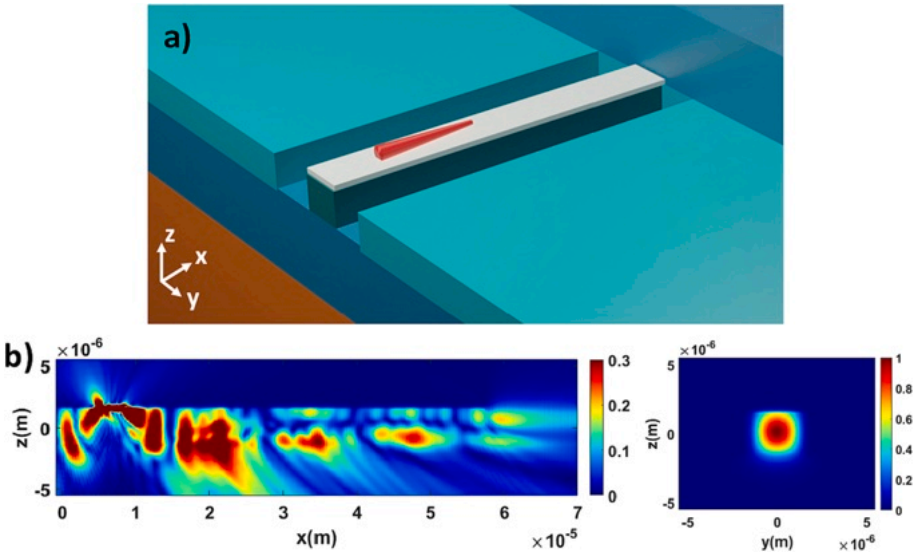

Fig. 14. a) Artistic representation of the exposed ridge waveguide to air, b) Electric field distribution along the propagation axis for a distance of 70 μm. Typical field of the waveguide's supported TE mode.

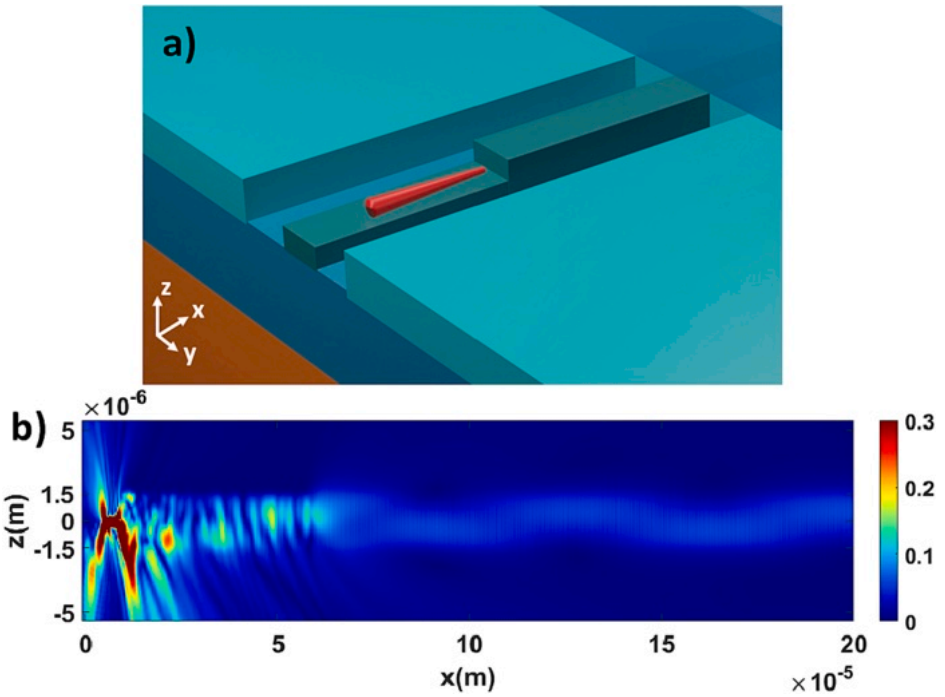

Fig. 15. a) Illustration of the NWQD in line to the ridge waveguide, b) Electric field distribution along the propagation axis of a 3 μm × 3 μm ridge and channel waveguide with NWQD inline.

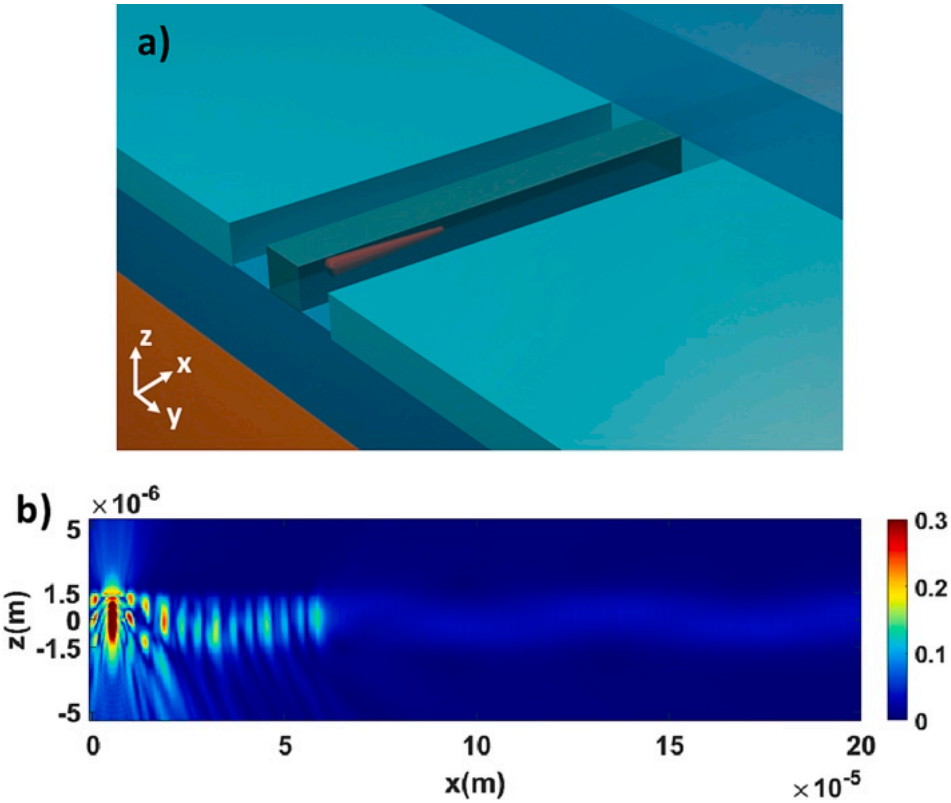

Fig. 16. a) Illustration of the NWQD embedded the ridge waveguide, b) Electric field distribution along the propagation axis of a 3 μm × 3 μm ridge and channel waveguide with NWQD embedded.

situation with laser-written waveguides it cannot be achieved high enough refractive index modification, limiting their performance to < 4% of coupling efficiency.

On the grounds of that limitation, the 3-layer silica-on-silicon photonics platform was explored as a viable solution, providing flexibility in tailoring the refractive index of the Ge-doped photosensitive core layer by selective doping and post-processing with direct UV writing to achieve an adequate degree of NWQD coupling suitable for

practical implementations. Accordingly, numerous arrangements were studied in terms of NWQD positioning and coupling into the channel waveguide. The evanescent coupling where the NWQD lays on top of a high refractive index dielectric layer above the channel waveguide was found incapable of transferring enough energy into the waveguide. Similarly, in the case where a part of the buried channel waveguide is exposed to air, the NWQD was designed and placed in various arrangements with the resulted ridge waveguide with higher confinement. However, surprisingly, the coupling was very low and no improvement was detected.

Finally, in an inline arrangement, the design issues and fabrication requirements for the precise positioning of the NWQD on the silica-on-silicon chip were discussed, demonstrating an adequate coupling efficiency with the potential for selectively inscribing Bragg grating reflectors to enhance the NWQD coupling even further. The inline-aligned arrangement was proved to be the simpler and more efficient while could allow for further optimization by proper adiabatic transformation through waveguide's appropriate shaping.

While challenges and limitations have been identified it is clear that new architectures for efficient coupling of NWQD in such silica based waveguides are currently required for enabling the fabrication of tailor-made laser written integrated optical circuits for scalable quantum computing applications. The coupling performance predicted by simulations can be significantly deteriorated by various material uncertainties, and fabrication imperfections, such as misalignments, in real implementation, and therefore new, robust architectures are necessary. Such new approaches have been identified, are currently under study, and will be reported in a future study.

Declaration of Competing Interest

The authors declare that they have no known competing financial interests or personal relationships that could have appeared to influence the work reported in this paper.

Data availability

Data will be made available on request.

Acknowledgements

This research work was funded by the Hellenic Foundation for Research and Innovation (H.F.R.I.) under the "First Call for H.F.R.I. Research Projects to support Faculty members and Researchers and the procurement of high-cost research equipment grant" (Project Number: HFRI-FM17-640, InPhoQuC).

References

[1] E. Knill, R. Laflamme, G.J. Milburn, A scheme for efficient quantum computation with linear optics, Nature 409 (6816) (2001) 46–52.
[2] J. Wang, F. Sciarrino, A. Laing, M.G. Thompson, Integrated Photonic Quantum Technologies, Nat. Photon. 14 (5) (2019) 273–284.
[3] G. Moody, V.J. Sorger, D.J. Blumenthal, P.W. Juodawlkis, W. Loh, et al., 2022 Roadmap on integrated quantum photonics, J. Phys. Photon. 4 (2022), 012501.
[4] M. Sartison, O. Camacho Ibarra, I. Caltzidis, D. Reuter, K.D. Jöns, Scalable integration of quantum emitters into photonic integrated circuits, Mater. Quantum Technol. 2 (2) (2022), 023002.
[5] B.J. Smith, D. Kundys, N. Thomas-Peter, P.G.R. Smith, I.A. Walmsley, Phase-controlled integrated photonic quantum circuits, Opt. Express 17 (16) (2009) 13516.
[6] S. Bogdanov, M.Y. Shalaginov, A. Boltasseva, V.M. Shalaev, Material Platforms for integrated quantum photonics, Opt. Mater. Express 7 (1) (2016) 111.
[7] H. Mahmudlu, R. Johanning, A. Kashi, A. van Rees, J. Epping, R. Haldar, K. Boller, M. Kues, Fully on-chip photonic turnkey quantum source for entangled qubit/Qudit State Generation, Nat. Photonics 17 (2023) 518–523.
[8] P. Senellart, G. Solomon, A. White, High-performance semiconductor quantum-dot single-photon sources, Nat. Nanotechnol. 12 (11) (2017) 1026–1039.
[9] Y. Arakawa, M.J. Holmes, Progress in quantum-dot single photon sources for Quantum Information Technologies: A broad spectrum overview, Appl. Phys. Rev. 7 (2) (2020), 021309.
[10] C.-Y. Lu, J.-W. Pan, Quantum-dot single-photon sources for the Quantum internet, Nat. Nanotechnol. 16 (12) (2021) 1294–1296.
[11] J. Claudon, J. Bleuse, N.S. Malik, M. Bazin, P. Jaffrennou, N. Gregersen, C. Sauvan, P. Lalanne, J.-M. Gérard, A highly efficient single-photon source based on a quantum dot in a photonic nanowire, Nat Photonics 4 (2010) 174–177.
[12] H. Mäntynen, N. Anttu, Z. Sun, H. Lipsanen, Single-photon sources with quantum dots in III–V nanowires, Nanophotonics 8 (5) (2019) 747–769.
[13] A. Jaffal, W. Redjem, P. Regreny, H.S. Nguyen, S. Cueff, X. Letartre, G. Patriarche, E. Rousseau, G. Cassabois, M. Gendry, N. Chauvin, InAs quantum dot in a needlelike tapered InP nanowire: A telecom band single photon source monolithically grown on Silicon, Nanoscale 11 (45) (2019) 21847–21855.
[14] M. Davanco, J. Liu, L. Sapienza, C.-Z. Zhang, J.V. De Miranda Cardoso, V. Verma, R. Mirin, S.W. Nam, L. Liu, K. Srinivasan, Heterogeneous integration for on-chip quantum photonic circuits with single quantum dot devices, Nat. Commun. 8 (1) (2017) 889.
[15] A. Orieux, M.A. Versteegh, K.D. Jöns, S. Ducci, Semiconductor devices for entangled photon pair generation: A Review, Rep. Prog. Phys. 80 (7) (2017), 076001.
[16] A.W. Elshaari, W. Pernice, K. Srinivasan, O. Benson, V. Zwiller, Hybrid integrated quantum photonic circuits, Nat. Photonics 14 (5) (2020) 285–298.
[17] I.E. Zadeh, A.W. Elshaari, K.D. Jöns, A. Fognini, D. Dalacu, P.J. Poole, M.E. Reimer, V. Zwiller, Deterministic integration of single photon sources in silicon based photonic circuits, Nano Lett. 16 (4) (2016) 2289–2294.
[18] I. Mnaymneh, D. Dalacu, J. McKee, J. Lapointe, S. Haffouz, J.F. Weber, D. B. Northeast, P.J. Poole, G.C. Aers, R.L. Williams, On-chip integration of single photon sources via evanescent coupling of tapered nanowires to sin waveguides, Adv. Quantum Technol. 3 (2) (2019) 1900021.
[19] A. Politi, M.J. Cryan, J.G. Rarity, S. Yu, J.L. O'Brien, Silica-on-silicon waveguide quantum circuits, Science 320 (5876) (2008) 646–649.
[20] I.J. Sparrow, P.G. Smith, G.D. Emmerson, S.P. Watts, C. Riziotis, Planar Bragg grating sensors—fabrication and applications: A Review, J. Sens. 2009 (2009) 607647.
[21] I. Liu, Z. Zhang, C. Flueraru, X. Liu, S. Chang, C.P. Grover, Waveguide shaping and writing in fused silica using a femtosecond laser, IEEE J. Sel. Top. Quantum Electron. 10 (1) (2004) 169–173.
[22] S.I. Tsintzos, K. Tsimvrakidis, A. Sinani, A. Bogris, J.C. Gates, P.G. Smith, A. W. Elshaari, V. Zwiller, C. Riziotis, Design and Fabrication Challenges of Integrated Optical Circuits for Quantum Computing Applications, in: 2023 23rd International Conference on Transparent Optical Networks (ICTON), IEEE, 2023, pp. 1–4.
[23] M.E. Reimer, G. Bulgarini, N. Akopian, M. Hocevar, M.B. Bavinck, M.A. Verheijen, E.P.A.M. Bakkers, L.P. Kouwenhoven, V. Zwiller, Bright single-photon sources in bottom-up tailored nanowires, Nat. Commun. 3 (1) (2012) 737.
[24] G. Corrielli, A. Crespi, R. Osellame, Femtosecond laser micromachining for integrated quantum photonics, Nanophotonics 10 (15) (2021) 3789–3812.
[25] K. Kalli, C. Riziotis, A. Posporis, C. Markos, C. Koutsides, S. Ambran, A.S. Webb, C. Holmes, J.C. Gates, J.K. Sahu, P.G.R. Smith, Flat fibre and femtosecond laser technology as a novel photonic integration platform for optofluidic based biosensing devices and lab-on-chip applications: Current results and future perspectives, Sens. Actuators B 209 (2015) 1030–1040.
[26] C. Riziotis, M.N. Zervas, Design considerations of optical add-drop filters based on grating assisted mode conversion in null couplers, IEEE/OSA, J. Lightwave Technol. 19 (1) (2001) 92–104.